
 Cite this: *RSC Adv.*, 2023, **13**, 2768

Adsorptive properties and on-demand magnetic response of lignin@Fe₃O₄ nanoparticles at castor oil–water interfaces†

 Mohammad Jahid Hasan,^{†a} Emily Westphal,^{‡b} Peng Chen,^b Abhishek Saini,^c I-Wei Chu,^d Sarah J. Watzman,^{id c} Esteban Ureña-Benavides^{id a} and Erick S. Vasquez^{id *be}

Lignin@Fe₃O₄ nanoparticles adsorb at oil–water interfaces, form Pickering emulsions, induce on-demand magnetic responses to break emulsions, and can sequester oil from water. Lignin@Fe₃O₄ nanoparticles were prepared using a pH-induced precipitation method and were fully characterized. These were used to prepare Pickering emulsions with castor oil/Sudan red G dye and water at various oil/water volume ratios and nanoparticle concentrations. The stability and demulsification of the emulsions under different magnetic fields generated with permanent magnets (0–540 mT) were investigated using microscopy images and by visual inspection over time. The results showed that the Pickering emulsions were more stable at the castor oil/water ratio of 50/50 and above. Increasing the concentration of lignin@Fe₃O₄ improved the emulsion stability and demulsification rates with 540 mT applied magnetic field strength. The adsorption of lignin@Fe₃O₄ nanoparticles at the oil/water interface using 1-pentanol evaporation through Marangoni effects was demonstrated, and magnetic manipulation of a lignin@Fe₃O₄ stabilized castor oil spill in water was shown. Nanoparticle concentration and applied magnetic field strengths were analyzed for the recovery of spilled oil from water; it was observed that increasing the magnetic strength increased oil spill motion for a lignin@Fe₃O₄ concentration of up to 0.8 mg mL⁻¹ at 540 mT. Overall, this study demonstrates the potential of lignin-magnetite nanocomposites for rapid on-demand magnetic responses to externally induced stimuli.

Received 13th December 2022

Accepted 9th January 2023

DOI: 10.1039/d2ra07952f

rsc.li/rsc-advances

1. Introduction

Nanoparticle adsorption at liquid–liquid interfaces plays a pivotal role in stabilizing Pickering emulsions and foams, with applications in targeted drug delivery, oil recovery, dye degradation, magnetic nanofluids, Pickering emulsions, and liquid–liquid extraction processes.^{1–10} Recent advancements in synthetic chemistry for the development of multi-responsive nanoparticles allow on-demand responses including interfacial adsorption–desorption capabilities, making magnetic

nanoparticles very useful in separation technologies.^{11–13} For example, functionalized magnetic carbonyl iron particles allow the preparation of Pickering emulsions with controllable stability and on-off demulsification properties.¹⁴ In another study, functionalized cellulose capped Fe₃O₄ nanofluids were utilized for the removal of methylene blue.¹⁵ Furthermore, nanoparticles enable the management of large-scale oil spills by dispersing spilled oil in water, gelling the oil, adsorbing the oil into porous sponges, or restricting the oil into thick slicks that allow on-demand separation.^{16,17} Hence, functionalized magnetic nanoparticles can be used in Pickering emulsions and oil recovery to achieve on-demand magnetically-driven separations.^{5,7,14,18}

Over the past few decades, magnetite (Fe₃O₄) nanoparticles have become the most common magnetic iron oxide nanoparticles (IONPs) studied due to their unique properties and increasing demand for magnetic fluids for biological, biomedical, environmental applications, and separation technologies.^{6,7,15,19–22} Fe₃O₄ nanoparticles are simple to synthesize at a reasonable cost and are significantly less hazardous than other magnetic nanoparticles.²³ However, for many applications, these must satisfy critical physical criteria, including colloidal and chemical stability, *i.e.*, resistance to

^aDepartment of Biomedical Engineering and Chemical Engineering, The University of Texas at San Antonio, One UTSA Circle, San Antonio, 78249, TX, USA

^bDepartment of Chemical and Materials Engineering, University of Dayton, 300 College Park, Dayton, OH, 45469-0256, USA. E-mail: evasquez1@udayton.edu

^cDepartment of Mechanical and Materials Engineering, University of Cincinnati, 2901 Woodside Drive, Cincinnati, OH, 45221, USA

^dInstitute of Imaging and Analytical Technology, Mississippi State University, Mississippi State, MS, 39762, USA

^eIntegrative Science and Engineering Center, University of Dayton, 300 College Park, Dayton, OH, 45469, USA

† Electronic supplementary information (ESI) available. See DOI: <https://doi.org/10.1039/d2ra07952f>

‡ 1st co-authors.



agglomeration and oxidation,^{6,24} as well as maintaining a high magnetization response. Therefore, in most applications, to increase colloidal and chemical stability and allow for further functionalization, Fe₃O₄ act as core materials coated and passivated with stabilizers, producing core-shell structures.^{7,25,26} Specific shell materials can include other metals, inorganic compounds, biomolecules, organic polymers, or monomers. Several studies have shown that coating with stabilizers can change the size, shape, and magnetism of Fe₃O₄.^{27,28} The functionalized superparamagnetic Fe₃O₄ nanoparticles (NPs) have potential applications in biomedical, biological, environmental, and separation technologies, especially in magnetically-controlled Pickering emulsions and oil spill separation.^{5,19,21,29}

Lignin can be used as an organic polymer to coat Fe₃O₄ NPs to increase the resistance to oxidation and improve colloidal stability and potential applications. Because of its biocompatibility, lignin is a good precursor for synthesizing environmentally friendly functional nanomaterials.³⁰ Lignin is the second most abundant biopolymer from plant-based sources; it is also cheap and non-toxic.^{31,32} Lignin has been used as antioxidant materials,³³ resins,³⁴ composites reinforcement,³⁵ biomaterials and tissue engineering,³⁶ carbon fibers precursors,³⁷ energy storage,³⁸ and antimicrobial agents.³⁹

Lignin-based nanoparticles have been used in stabilizing Pickering emulsions and oil herding in literature for various applications.^{40–43} Dai *et al.* used lignin-based nanoparticles to stabilize Pickering emulsions for the emulsion stability improvement and thermal-control release of *trans*-resveratrol.³⁹ Wang *et al.* developed lignin-based Pickering emulsion as a polymerization reaction medium to prepare microencapsulate 1-tetradecanol.⁴² Pang *et al.* developed lignin/sodium dodecyl sulfate composite NPs and applied them in Pickering emulsion for template-based microencapsulation.⁴¹ In another study, lignin based NPs were used as stabilizer for Pickering emulsions to obtain antibacterial phase change microcapsule.⁴⁰ Moreover, magnetic NPs have been found to be useful in stabilizing Pickering emulsions because of their adsorptive properties on oil-water interface.^{43–45} Iron oxide nanoparticles are typically used to stabilize the emulsions, while Wang *et al.* used carbon nanotube/iron oxide hybrid nanoparticles.⁴³ Dudchenko *et al.* created magnetic oil/water Pickering emulsions stabilized by Fe nanoparticles in a variety of ionic strength environments where the continuous aqueous phase was separated through a superoleophobic membrane, while high emulsion stability prevented oil droplet coalescence and consequential membrane fouling.⁴⁴ The magnetic Fe nanoparticles were then recovered by the action of a magnet.⁴⁴ Kim *et al.* studied polymerized polystyrene/Fe₂O₃ composite particles-stabilized Pickering emulsions and their magnetoresponsive characteristics.⁴⁵ Moreover, Lee *et al.* (2018) studied the efficacy of lignin nanoparticles at oil-water interface as an ecofriendly alternative to oil spill recovery.⁴⁶ When conventional molecular oil herding agents desorb from the interface and herded oil lack stability, they found that the lignin nanoparticles provided long term stability of the herded oil and made sure complete removal of the herded oil when they were used in a mixture of aqueous solution and alcohol.

In previous studies, there are only a few examples of magnetic nanoparticles and lignin-based hybrid materials where lignin particles have been used in various applications, particularly in chemical separation processes.^{47,48} Petrie *et al.* synthesized kraft lignin coated Fe₃O₄ nanocomposites by using pH driven separation techniques and studied the effect of lignin content on the properties of hybrid lignin@Fe₃O₄. A recent study found that magnetic lignin spheres adsorb methylene blue and rhodamine B, both of which are model organic dyes that could be found in wastewater.⁴⁸ Kolodynska *et al.* report that nanoparticle concentration, solution pH, and interaction time improve heavy metal adsorption using lignin/Fe₃O₄ hybrid.⁴⁹ These studies highlight the superior properties of the magnetic lignin nanocomposites for removal of pollutants as compared to each individual nanomaterial. Hence, we hypothesize that lignin-based nanocomposites have potential applications in magnetically-controlled Pickering emulsions.

In this work, we demonstrate the adsorptive and magnetic properties of lignin@Fe₃O₄ in castor oil-water interface as an environmentally friendly stabilizer for magnetically-controllable Pickering emulsions and oil-herding. The effect of nanoparticle concentrations and the effect of different magnetic field on emulsion stabilization and demulsification was studied. Moreover, we studied lignin@Fe₃O₄ as a magnetically-controllable herding agent for castor oil spill recovery by dispersing them in water, followed by adding an oil spill on water surface and then alcohol (1-pentanol) to the water. We found that lignin@Fe₃O₄ nanocomposites adsorbed to oil-water interface and herded the oil spill with the use of simple external permanent magnets with different magnetic fields.

2. Materials and methods

2.1 Materials

Iron(II) chloride (98%), iron(III) chloride (97%), ammonium hydroxide solution (28–30%), sodium hydroxide solution (50%), Kraft Lignin (alkali), Sudan Red G dye, and castor oil were supplied by Sigma-Aldrich (USA). Ultrapure water (Type I) was obtained from an EMD water purification system (MilliporeSigma). 1-Pentanol (71-41-0) was used and supplied by TCI (USA), and absolute ethanol (64-17-5) and methanol (67-56-1) were both supplied by Fisher Chemical. Two different Neodymium N42 permanent magnets (Applied Magnets, TX) were used, one with dimensions 0.5 × 0.5 × 2 inches and the other 1 × 1 × 2 in, generating magnetic fields of 540, 370, 100, and 5 mT, which were measured using a PCE-MFM 3000-ICA magnetometer (PCE instruments, UK). Labnet BioPette Plus Volume Pipette and tips were supplied from Steller Scientific. All chemicals were used as received and without further purification.

2.2 Synthesis and characterization of Fe₃O₄ and lignin@Fe₃O₄ nanoparticles

A co-precipitation method was used to synthesize a large batch of Fe₃O₄ nanoparticles based on a slightly modified Massart method⁵⁰ and Petrie's method.^{47,51} Lignin@Fe₃O₄ nanoparticles



were prepared using a 3 : 1 mass ratio of kraft lignin (KL) to magnetite. Specific details about the synthesis and multiple characterization techniques employed in this work are described in Sections ESI 1–3.†

2.3 Emulsions without nanoparticles

Sudan red G dye was added to castor oil (CO) at a concentration of 0.60 mg mL^{-1} and used for all emulsions. The emulsions without nanoparticles were made by adding pure water and the dyed CO using an Eppendorf pipette in the following volumetric ratios: 10/90, 30/70, 50/50, 70/30, and 90/10 (oil/water).²⁹ All emulsions were 10 mL total, made in glass vials, and repeated 3 times total. A Turrax T-25 high shear mixer was used to emulsify the oil/water mixtures for 5 minutes at 13 000 RPM. To avoid the temperature of the emulsion from rising, all vials were placed in a water bath during high shear mixing. After high shear mixing, small amounts of sample from the middle/top and bottom layers were added to a Petri dish full of CO and a Petri dish full of water to determine if the emulsions were oil-in-water (O/W) or water-in-oil (W/O), called the drop test method.⁵² Pictures of the emulsions were taken 0 min, 15 min, 30 min, 1 hour, 24 hours, and 1 month after being high sheared.²⁹ Both layers of the emulsions were looked at $10\times$, $20\times$, and $50\times$ using an Axio Vert. A1 Inverted Reflected Light Microscope after 0 min, 30 min, and 24 hours of high shearing and droplet sizes were measured using the ImageJ software at $50\times$.⁵¹ 300 total droplet sizes were measured per emulsion.

2.4 Pickering emulsions stabilized by lignin@Fe₃O₄ nanocomposites

Pickering emulsions (with NPs) were made using a similar procedure as the emulsions without nanoparticles, except an aqueous NP solution was added to the water phase before high shear mixing. 10/90 control emulsion was very unstable without nanoparticles, so it was not repeated for the Pickering emulsions. Three different nanoparticle concentrations were used: 0.1 w/v%, 0.5 w/v%, and 1.0 w/v%.²⁹ The 30/70 ratio was first made using the 1.0 w/v% NP concentration and did not stay emulsified long, so it was also not repeated. Therefore, the three main ratios made in this section were 50/50, 70/30, and 90/10, all tested at the three NP concentrations.

To start, 1 wt%, 5 wt%, and 10 wt% NP suspensions were made to be used for the 0.1 w/v%, 0.5 w/v%, and 1.0 w/v% NP concentration emulsions, respectively. Each of the suspensions were placed in an ultrasonicator bath (Branson, M5800) for 20 minutes. Then, 1 mL from each wt% suspension was added to the corresponding w/v% emulsion and combined with the remaining water needed for the specific oil/water ratio. The CO/Sudan Red G dye was then added on top of the aqueous NP phase in the glass vial and was high sheared at 13 000 RPM for 5 minutes. The drop test method was performed on samples taken from the middle and bottom of the emulsion, and pictures were taken at 0 min, 2 min, 15 min, 30 min, 1 hour, 24 hours, and 48 hours. Microscopy images were also taken at 0 min, 30 min, and 24 hours at $10\times$, $20\times$, and $50\times$, and droplet sizes were measured using the ImageJ software.

The magnetic demulsification process was tested on the lignin@Fe₃O₄ Pickering emulsions at different magnetic fields: 540 mT, 370 mT, 100 mT, and 5 mT. After the drop test method was performed, each emulsion was placed a certain distance away from one of the two neodymium N42 permanent magnets. The 540 mT magnetic field was achieved by placing the emulsion directly on the N42 medium magnet ($0.5 \times 0.5 \times 2$ in). The 370 mT, 100 mT, and 5 mT were achieved by placing the emulsion on 0.5 cm, 2.5 cm, and 8.5 cm, respectively, from the N42 large magnet ($1 \times 1 \times 2$ in). The distances were measured using a ruler and the magnetic field was measured with a PCE-MFM 3000-ICA magnetometer. Along with the four emulsions exposed to a magnetic field, an additional emulsion was not exposed to a magnetic field (0 mT), where the stability of the Pickering emulsion was observed over time. All emulsions were taken off the magnet after 48 hours, and photographs were taken after 1 week for each emulsion.

2.5 Oil herding using lignin@Fe₃O₄ nanocomposites and 1-pentanol

The procedure for this section was a modified version of the Lee *et al.* methodology.⁴⁶ Three nanoparticle-loaded suspensions were made: 0.75, 0.80, and 0.85 mg mL^{-1} . Five mL of pure water were placed in a glass vial using an Eppendorf pipette, and the corresponding concentration of lignin@Fe₃O₄ nanoparticles were added to the vial. The suspensions were placed in an ultrasonicator bath for 15 minutes to ensure full dispersion. Using the pipette, a 9 : 1 ratio was made using 0.9 mL of the aqueous NP solution previously prepared and 0.1 mL of 1-pentanol. The mixture was swirled by hand for ~ 10 seconds to mix the two liquids. First, 10 mL of pure water was added to a small, plastic Petri dish (diameter: 5.5 cm), followed by the 9 : 1 mixture. Then, 0.05 mL of Castor Oil/Sudan Red G dye was added at the center of the dish. Pictures of the dish were taken immediately after the oil was added (0 minutes), 2 min, 5 min, 10 min, 20 min, and 1 hour after. Using the medium sized N42 rare earth magnet ($0.5 \times 0.5 \times 2$ inches) with a magnetic field of ~ 540 mT (at 0 cm) and the large N42 rare earth magnet ($1 \times 1 \times 2$ in) with a magnetic field of 425 mT (at 0 cm), the oil droplet was manipulated at 0 min. Video was used to record this phenomenon to compare the velocity of the herded oil at the different magnetic fields. (Note: the medium magnet had a magnetic field of 13 mT at the center of the Petri dish (radius: 2.75 cm) and the large magnet had a magnetic field of 60 mT at the center). This process was repeated 3 times total for each NP concentration. A control run was also done using just water and CO/dye to see how long the oil stays herded over time without nanoparticles or alcohol. The diameters of the herded oil were measured using the ImageJ software at each of the times when the pictures were taken.

2.6 Statistical analysis

Quantitative data are expressed as mean \pm standard deviation/error of the mean. Emulsion droplet size comparisons were done using an ANOVA *t*-test on Excel to determine statistical differences.



3. Results and discussion

3.1 Characterization of kraft lignin and lignin@Fe₃O₄ nanocomposites

Lignin@Fe₃O₄ NPs were characterized using a variety of experimental techniques. Fig. 1a shows the TEM images of Lignin@Fe₃O₄, confirming a multicore-shell nanostructure, where multiple IONPs are encapsulated with a lignin shell.⁴⁷ The average size of IONPs was found to be 13.4 ± 5.5 nm.

TGA was used to determine the thermal stability of lignin@Fe₃O₄, KL, and neat Fe₃O₄ nanoparticles, as well as the amount of KL grafted onto the magnetite nanoparticles. Fig. 1b depicts the percent weight loss of each sample as temperature increased. It was determined that lignin@Fe₃O₄ lost ~13% of

its total weight as temperature approached 800 °C, whereas KL lost ~62%, and neat Fe₃O₄ lost less than 1%. This result demonstrates that magnetite has high thermal stability, as compared to KL. Most of the weight loss of KL occurred between 200–400 °C. For the lignin@Fe₃O₄ nanoparticles, some weight loss occurred between 25–200 °C, which could be attributed to excess adsorbed moisture. Furthermore, lignin@Fe₃O₄ lost some weight between 200 °C to 750 °C due to the lignin decomposition before reaching a plateau at 750 °C. The amount of KL coating on the IONPs was determined using ESI eqn S1† (final weight at 781 °C) and was calculated to be 21.43%.

FT-IR spectroscopy of lignin@Fe₃O₄ was obtained and compared with the FT-IR spectra of neat IONPs and KL. The FT-IR spectrum for the neat IONPs has very few peaks compared to

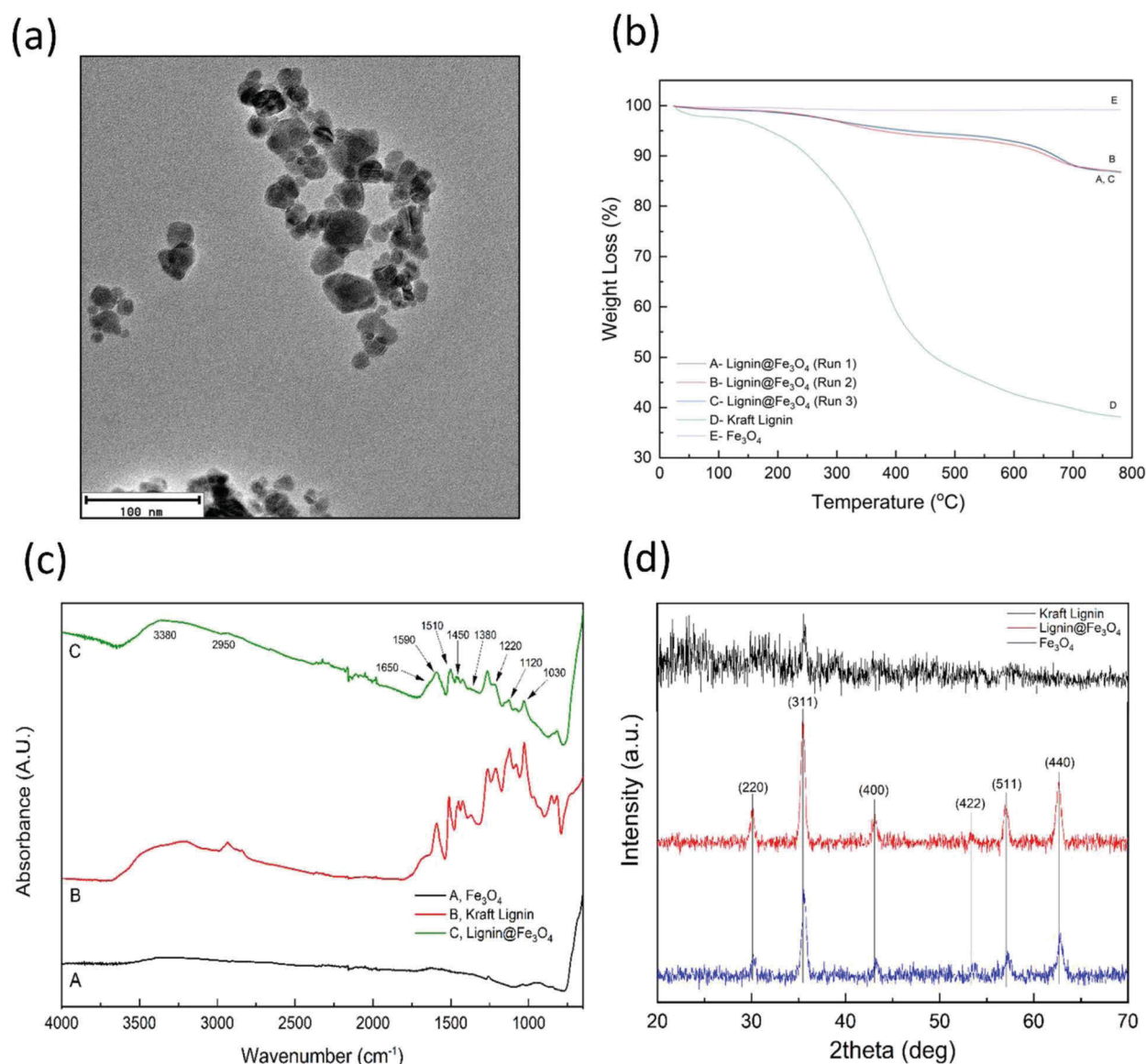


Fig. 1 Characterizations of neat Fe₃O₄, kraft lignin, and lignin@Fe₃O₄. (a) TEM images of lignin@Fe₃O₄; (b) TGA results for lignin@Fe₃O₄ (A–C), KL (D), and neat Fe₃O₄ nanoparticles (E); (c) FT-IR spectra of neat Fe₃O₄, kraft lignin (KL), and lignin@Fe₃O₄ nanoparticles; (d) XRD spectra for kraft lignin (black), lignin@Fe₃O₄ (red), and neat Fe₃O₄ (blue) powder samples. The numbers in the parenthesis represent the Miller indices at each of the Bragg reflections (peaks).



KL and coated magnetic nanoparticles (Fig. 1c). Neat IONPs showed characteristic Fe_3O_4 peaks at 3380 and 1650 cm^{-1} corresponding to hydroxyl groups ($-\text{OH}$) and $\text{O}-\text{H}$ scissoring, respectively.⁴⁷ On the contrary, the KL spectrum had many peaks in the fingerprint region ($400\text{--}1500\text{ cm}^{-1}$), demonstrating the structural intricacy of this biobased polymer.⁵³ The characteristic peaks of KL at 1030 cm^{-1} and 1120 cm^{-1} were assigned to $\text{C}-\text{O}$ deformation and aromatic $\text{C}-\text{H}$ formation, respectively. The characteristic peak at 1220 cm^{-1} was due to $\text{C}-\text{C}$, $\text{C}-\text{O}$, and $\text{C}=\text{O}$ stretching. Furthermore, additional peaks of KL at 1380 , 1450 , 1510 , 1590 , 1650 and 2950 cm^{-1} corresponded to $\text{C}-\text{C}$ stretching, $\text{C}=\text{C}$ stretching in aromatic rings, $\text{C}-\text{C}$ stretching of aromatic bonds, aromatic vibrations, conjugated carboxyl group, and stretching vibrations of $\text{C}-\text{H}$ bonds, respectively.^{47,51,53} The spectrum for $\text{lignin}@Fe_3O_4$ shared many of the same peaks as the KL spectrum, however, there was a slight blue-shift at 1650 cm^{-1} compared to neat KL, possibly due to the bound hydroxyl groups between the lignin and iron oxide.⁵⁴

XRD spectra was obtained for kraft Lignin, $\text{lignin}@Fe_3O_4$, and neat IONP powder samples. The 2-theta degrees at which the peaks occurred for $\text{lignin}@Fe_3O_4$ and Fe_3O_4 (Fig. 1d) demonstrated the primary Bragg reflections, located at 30° , 35° , 43° , 53° , 57° , 63° , that corresponded to the face-center cubic (FCC) Miller indices of (220), (311), (400), (422), (511), and (440) of Fe_3O_4 nanoparticles, respectively.^{47,51,55} The neat IONPs and $\text{lignin}@Fe_3O_4$ had the same six peaks, while the KL spectrum only shared one peak at 35° . Using the Scherrer Equation (ESI eqn (S2)†), the crystallite size of the $\text{lignin}@Fe_3O_4$ nanoparticles at 35° was determined to be 18.4 nm (ESI eqn (S2)†) since the FWHM was 0.009234 radians and the Bragg diffraction angle was 0.61897 radians.

$\text{lignin}@Fe_3O_4$ nanoparticles were also analyzed using zeta potential and DLS (ESI, Fig. S1†). The zeta potential of

$\text{lignin}@Fe_3O_4$ was found to be -0.04 V (-40 mV) as shown in Fig. S1a,† implying that the particles are colloidal stable with the potential to interact with positively charged surfaces.^{56,57} The high zeta potential (-40 mV) of $\text{lignin}@Fe_3O_4$ resulted in a high electrostatic particle-particle repulsion. The hydrodynamic diameter, referred to as effective diameter (D_{eff}) in Fig. S1b,† and the number average diameter ($D_{\#}$) of the $\text{lignin}@Fe_3O_4$ were determined by DLS. The D_{eff} of $\text{lignin}@Fe_3O_4$ was calculated with the Stokes-Einstein equation (ESI eqn (S3)†),⁵⁸ and was found to be $168 \pm 1.7\text{ nm}$, while the number average diameter ($D_{\#}$) was calculated to be $98.75 \pm 25\text{ nm}$ (Fig. S1b†). Additionally, a polydispersity of 0.236 was obtained for the $\text{lignin}@Fe_3O_4$, indicating some aggregation and the multimodal particle size distributions.

The magnetic properties of $\text{lignin}@Fe_3O_4$ showed a saturation magnetization of $\sim 50\text{ emu g}^{-1}$ at 300 K . The IONPs without lignin coating had a value of $\sim 65\text{ emu g}^{-1}$ at 300 K (Fig. 2a). At a relatively low applied magnetic field (1000 Oe), the nanoparticles' magnetization increased linearly from 0 to 25 K for both neat Fe_3O_4 and $\text{lignin}@Fe_3O_4$, and then curve to a broad maximum, followed by a slight drop. Under this condition, the maximum magnetization for $\text{lignin}@Fe_3O_4$ and neat Fe_3O_4 was determined to be $\sim 35\text{ emu g}^{-1}$ and $\sim 47\text{ emu g}^{-1}$, respectively. This result confirms the magnetic response of the nanoparticles at low magnetic field intensities (0.1 T), which is of interest for a rapid on-demand magnetic response, especially for demulsification processes. Since, the measurements are done on a per unit mass of sample basis, the saturation magnetization is expected to be lower for $\text{lignin}@Fe_3O_4$ compared to neat magnetite NPs due to the larger total mass of the NPs that include the non-magnetic lignin coating.²⁶

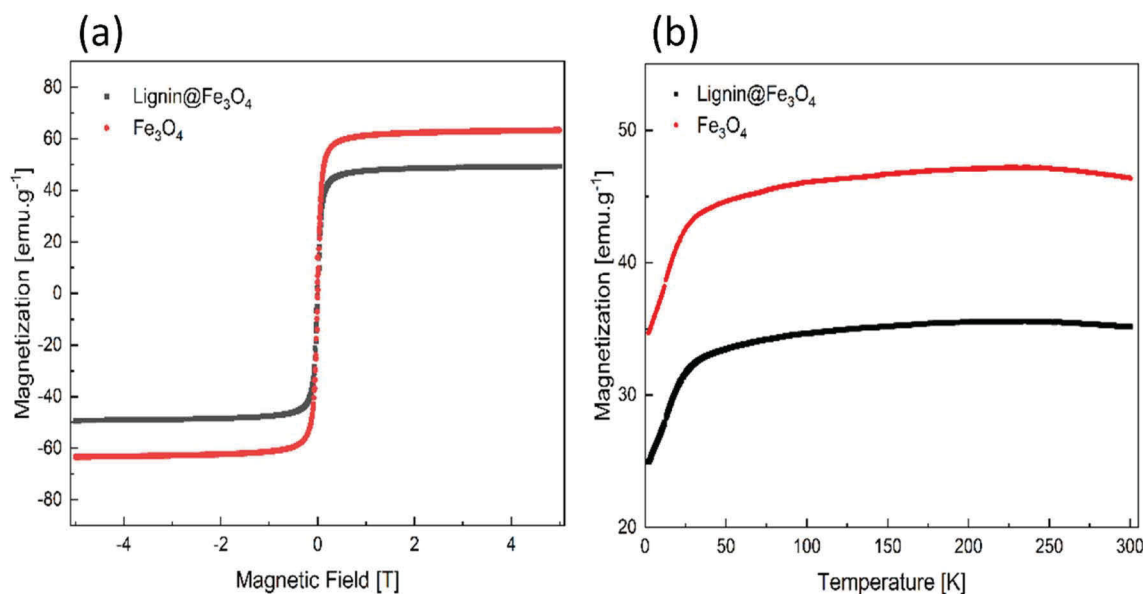


Fig. 2 Magnetization results for $\text{lignin}@Fe_3O_4$ and neat Fe_3O_4 nanoparticles. (a) Magnetic hysteresis loops for the two samples at 300 K ; (b) magnetization-temperature profile with a magnetic field strength of 1000 Oe .



3.2 Pickering emulsions stability and demulsification process over time

The stability of the castor oil–water emulsion prepared without nanoparticles was investigated first. As a control test, five oil/water ratios (10/90, 30/70, 50/50, 70/30, and 90/10) were emulsified without any lignin@Fe₃O₄ nanoparticles. Significant creaming occurred for the three lowest oil ratios (10/90, 30/70, and 50/50) (Fig. S2†). The emulsions prepared with castor oil to water volume ratios of 10/90 and 30/70 were seen to have phase separation immediately after high shearing, while the other three ratios (50/50, 70/30 and 90/10) were observed to have comparatively better emulsion stability providing less phase separation; nevertheless, they started breaking within a minute or two, indicating poor emulsion stability without nanoparticles. In all cases, two distinct layers formed, with the middle/top layer initially containing more water than oil and the bottom layer containing more oil. Fig. 1a and b shows the picture of the control emulsions for 50/50 and 70/30 oil/water ratios, respectively, at time 0 min, 30 min and 24 h.

The average droplet sizes of the control emulsions were determined from microscopy images of at least 300 droplets. The

emulsion samples were taken from the bottom layer (Fig. 3c) and top/middle layer (Fig. 3d) and were observed under an optical microscope at 0 min, 30 min, and 24 hours. The samples were taken from the two layers to investigate the variability of the droplet sizes in the different layers. The results showed that the middle layer was more watery at 0 minutes for most ratios; therefore, droplet sizes were smaller on average to start. The average droplet size and standard deviation increased as oil ratio increased for all oil to water ratios. The average sizes of the droplets for 10/90, 30/70, 50/50, 70/30, and 90/10 bottom layer emulsions were found to be $7.49 \mu\text{m} \pm 3.15 \mu\text{m}$, $8.59 \pm 2.88 \mu\text{m}$, $10.84 \pm \mu\text{m}$, $12.32 \pm 5.77 \mu\text{m}$, and $14.12 \pm 6.63 \mu\text{m}$, respectively, initially at 0 min. The average size of the emulsion droplets taken from the middle layer for various oil/water ratios followed the same trend, however, the average droplet size was smaller than the bottom layer in most oil/water ratios, however, it was smaller than for the bottom layer in most oil/water ratios. Because the 10/90 and 30/70 emulsion had the least stability without nanoparticles, these were not further investigated in this study.

In an effort to determine the effect of lignin@Fe₃O₄ nanoparticles on castor-oil/water Pickering emulsions stability, we

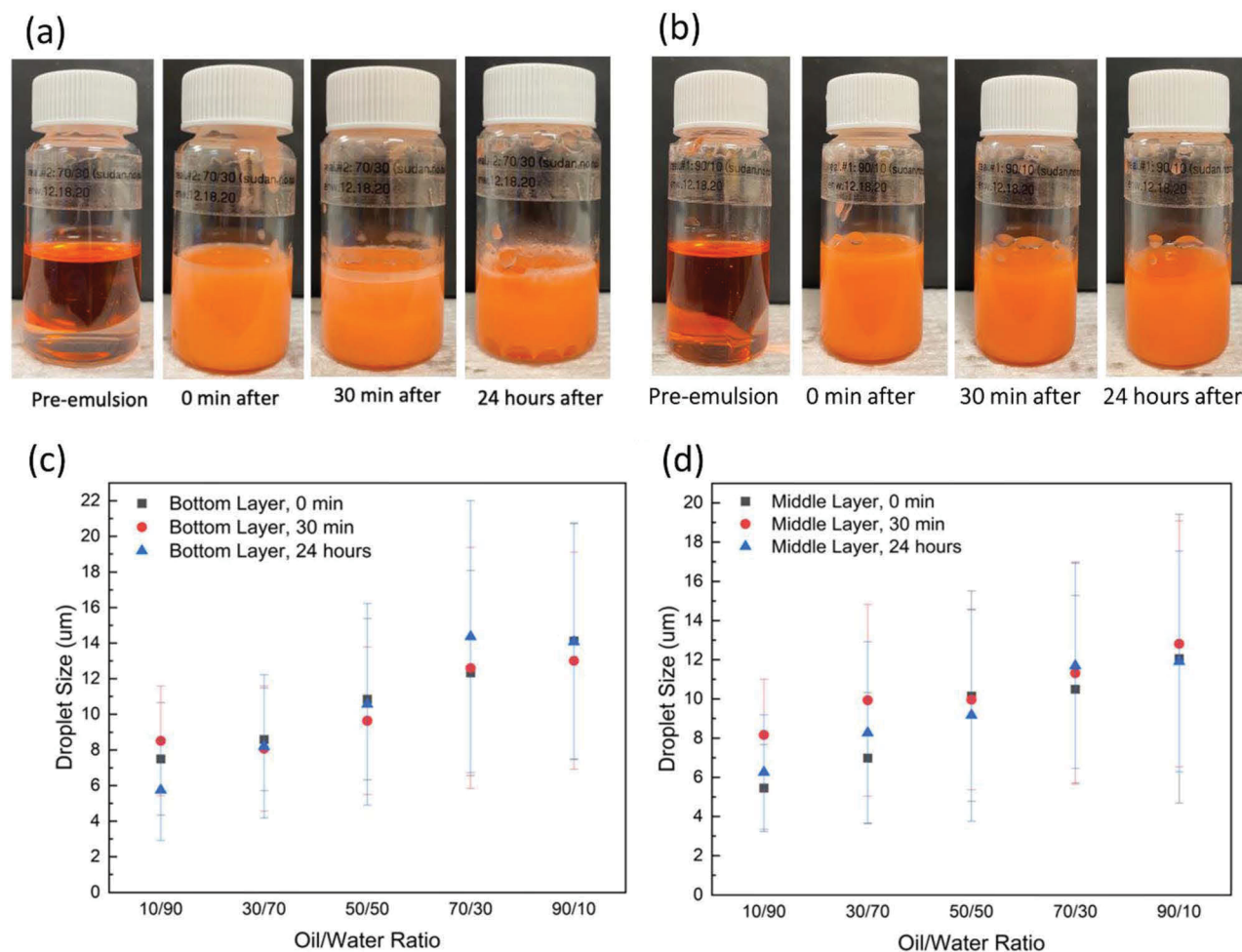


Fig. 3 Control emulsions prepared at castor oil to water volume ratio of (a) 50/50; (b) 70/30; average droplet size of the emulsions prepared at various oil/water ratios for the samples taken from (c) bottom layer of the emulsion vials; (d) samples taken from the middle layer.



analyzed 50/50, 70/30, and 90/10 castor-oil/water ratios and used three different NP concentrations (0.1, 0.5, and 1 w/v%). Images of 50/50 and 70/30 emulsions prepared at various concentrations of lignin@Fe₃O₄ are shown in Fig. 4. All of the emulsions were O/W based on the drop test method, performed similarly to Qiao *et al.*⁵⁹ Hence, if the NPs are dispersed in the water phase initially, the Pickering emulsions were O/W.⁴ The results showed that the emulsions with the highest nanoparticle concentrations stayed

emulsified the longest providing more nanoparticles at the interface, consistent with existing literature.⁶⁰ The 0.5 w/v% and the 1.0 w/v% NP concentrations showed better stability over time compared to 0.1 w/v%, and were also successfully demulsified in the presence of an external permanent magnet, especially at higher oil/water ratios. These results are similar to experiments done with cellulose nanocrystal (CNC)@Fe₃O₄ nanocomposites water ratios.²⁹

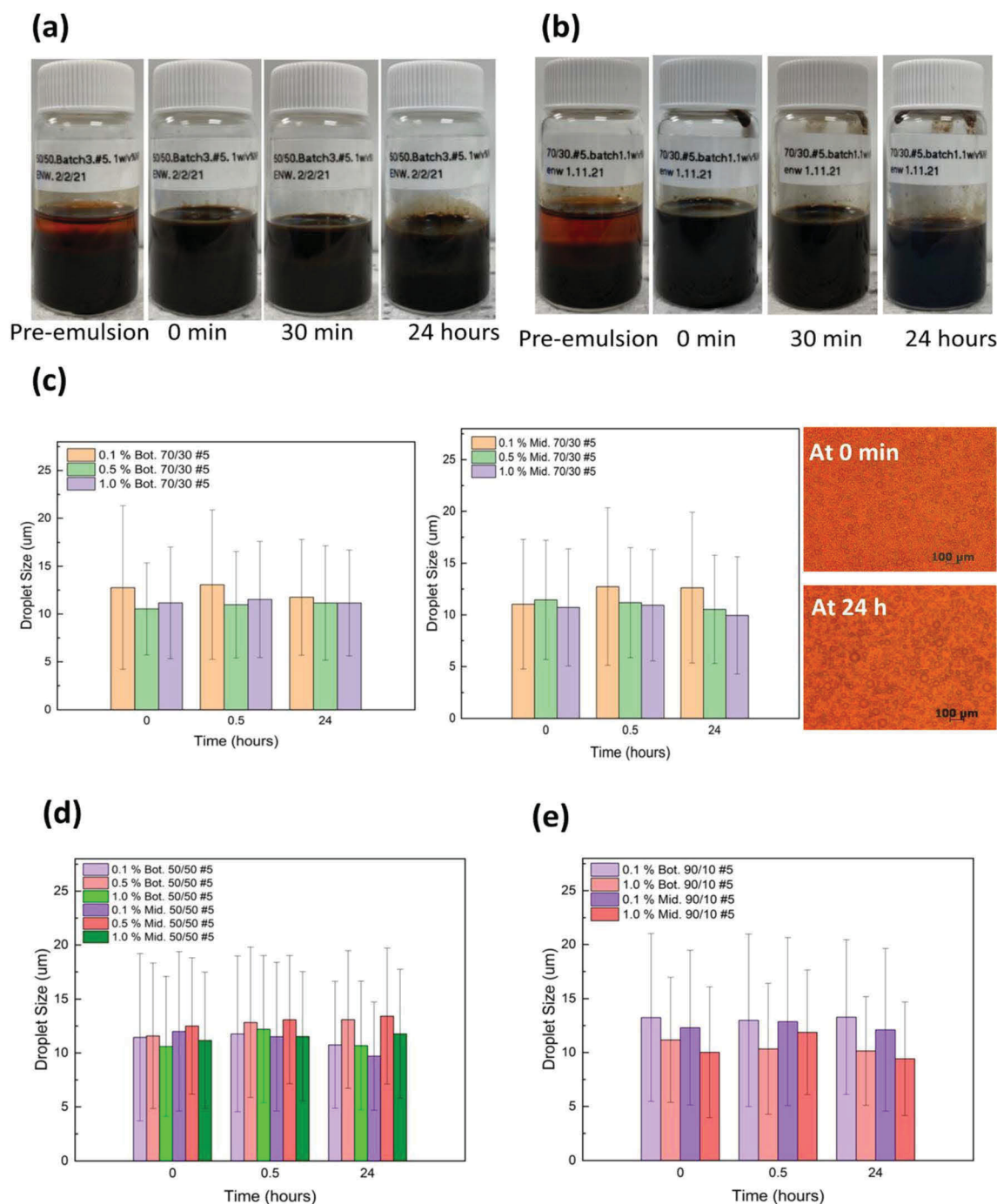


Fig. 4 Castor-oil/water (CO/W) Pickering emulsions stabilized with 1 w/v% lignin@Fe₃O₄ NPs at CO/W volume ratio of (a) 50/50; (b) 70/30; average droplet size of the emulsions stabilized at varied NPs concentration over 24 hours of both bottom layer and middle layer of the (c) 70/30; (d) 50/50; and (e) 90/10 emulsions; example optical microscopy images show the 70/30 emulsion droplets at time 0 h and after 24 h.



In terms of the oil-to-water ratio, the results showed that the 50/50 emulsions were less stable with two distinct phases forming after 24 hours, which contained primarily oil at the top and water in the bottom phase due to the water's higher density, yet both phases were still emulsified (Fig. 4a). The 70/30 emulsions exhibited the longest stability and had a dark brown color over 24 hours (Fig. 4b). Due to the low water content, at 0.5 wt% lignin@Fe₃O₄ the 90/10 emulsions did not remain emulsified for more than 24 hours (Fig. S3†).

The stability of the lignin@Fe₃O₄-stabilized Pickering emulsions was further assessed by examining the change in droplet size over a 24 hours period. It was discovered that for emulsions prepared with 70/30 CO/W ratio and 1.0 w/v% NP concentration, the droplet size remained almost unchanged over 24 hours in both bottom and top/middle layers (Fig. 4c). A *t*-test ($\alpha = 0.05$) revealed there was no discernible difference in the droplet size over time for either layer, indicating a high stability of the emulsions. Two micrographs of the middle layer of a 70/30, 1.0 w/v%, emulsion at 0 min and 24 hours are shown in an example (Fig. 4c). The 70/30 emulsions stabilized by 0.1 w/v% and 0.5 w/v% NPs were also found to be stable for 24 hours, with minor changes in droplet size over time. Likewise, the 50/50 emulsions at 0.1, 0.5, and 1.0 w/v% (Fig. 4d) and 90/10 emulsions at 0.1 and 1.0 w/v% (Fig. 4e) showed similar droplet size trends compared to 70/30, but they were not as stable over time and had higher standard deviations.

In our previous study, we successfully demulsified castor oil-water Pickering emulsions, stabilized by CNC@Fe₃O₄ NPs, by using a permanent magnet.²⁹ In this paper, the demulsification capability of the lignin@Fe₃O₄-stabilized emulsions was observed by applying different magnetic fields to the Pickering emulsions (540, 370, 100, and 5 mT). Fig. 5a and b shows the demulsification of 50/50 and 70/30 emulsions stabilized 1 w/v% NPs, respectively, at 540 mT. Fig. 5c shows the average sizes of the 70/30, 1 w/v%, emulsion droplets at 540 mT for a 24 hours period. For the 70/30 Pickering emulsions exposed to the strongest magnetic field (540 mT), the 0.5 and 1.0 w/v% NP concentrations emulsions separated into a clean middle layer, while for the bottom layer, only the 0.5 w/v% fully separated.

We attributed this event to competing effects of magnetic field strength inside the emulsion and nanoparticle adsorption at the oil/water interface. It is proposed that at very low NP concentrations, the overall magnetic field inside the emulsion is smaller; thus, at 0.1 w/v% the NPs cannot be pulled out of the interface by the lower internal field. On the other hand, at the higher, 1.0 w/v% NP concentration, the internal field is stronger allowing to pull more nanoparticles from the interface, yet the concentration is so large that some nanoparticles cluster as aggregates around the droplets and cannot be pulled away from the oil-water interface.

For all three NP concentrations, the droplet size decreased from 0 min to 24 hours, which was due to the breaking of large droplets over time, indicating a successful magnetically-induced demulsification process. At lower magnetic fields, the overall change in droplet size over time decreased, meaning the demulsification process was not as strong compared to 540 mT (Fig. 5e). The magnetic field of 5 mT provided very similar

results as 0 mT (no magnetic field), while 540 mT demulsified the emulsions into two clean layers. The 370 and 100 mT had results between that of 540 and 5 mT. Therefore, the results demonstrated that increasing the magnetic field improved the magnet's demulsification ability. Furthermore, when evaluating demulsification effectiveness on CO/W ratios, it was discovered that the 50/50 and 70/30 ratios at 540 mT had a more obvious separation than the 90/10 ratio for all NP concentrations (Fig. S4†), owing to the larger water content. After 24 hours, the 50/50 emulsions were successfully broken, and the two phases were separated while the middle layer was completely clear containing orange CO and the bottom layer was an aqueous light brown phase. No droplets were seen after 24 h in the middle layer under the microscope for 50/50 emulsions; hence, a 0 μ m bar (no bar) average size of the droplets is shown in Fig. 5d.

Although the 50/50 emulsions separated well, these showed the least stability over a 24 hours period without a magnetic field, which is why the 70/30 ratio was chosen as the most adequate oil/water ratio to obtain highly stable Pickering emulsions that can be broken by using a simple external permanent magnet. The lignin@Fe₃O₄ NP concentrations of 0.5 and 1.0 w/v% provided similar results in terms of demulsification at 540 mT, while 0.1 w/v% was unable to demulsify as cleanly as the other two NP concentrations possibly due to the low magnetic field inside the emulsion. Overall, the lignin@Fe₃O₄-stabilized Pickering emulsions, prepared at particular conditions (e.g. 70/30 CO/W ratio and 1 w/v% NPs) can provide good emulsion stability and on-demand demulsification capability given a sufficiently high magnetic field (e.g. 540 mT).

3.3 Lignin@Fe₃O₄ NPs in oil herding

Lignin@Fe₃O₄ NPs were further tested on oil herding experiment. Three different alcohols, *i.e.*, methanol, ethanol, and propanol, were tested to initiate Marangoni flow to herd the oil. The Marangoni effect occurs as a result of a surface tension gradient-driven flow,⁶¹ and requires a sufficiently heavy alcohol to initiate that flow.⁶² Ethanol and methanol were found to be unable to herd the oil at all, whereas 1-pentanol was able to herd the oil tightly for 60 minutes. The hydrophobic chains of ethanol and methanol are small compared to 1-pentanol's, meaning they most likely are not hydrophobic enough to carry the aqueous NP solution to the interface. Therefore, 1-pentanol was chosen as the alcohol used in the oil herding experiment. Fig. 6 shows the oil herding experiment and size of the herded oil over time for the control (no NPs), 0.75, 0.80, and 0.85 mg mL⁻¹ NP concentration. The results demonstrated that the control had the largest average oil diameter and standard error, while the 0.80 mg mL⁻¹ had the smallest. The control had the largest diameter since Marangoni flow is not possible without alcohol and nanoparticles, therefore the oil spread out widely over time. The 0.80 mg mL⁻¹ had the smallest diameter over time compared to 0.85 mg mL⁻¹ most likely due to the higher NP concentration being too heavy for the alcohol to carry it to the oil-water interface during the initial Marangoni flow (ESI



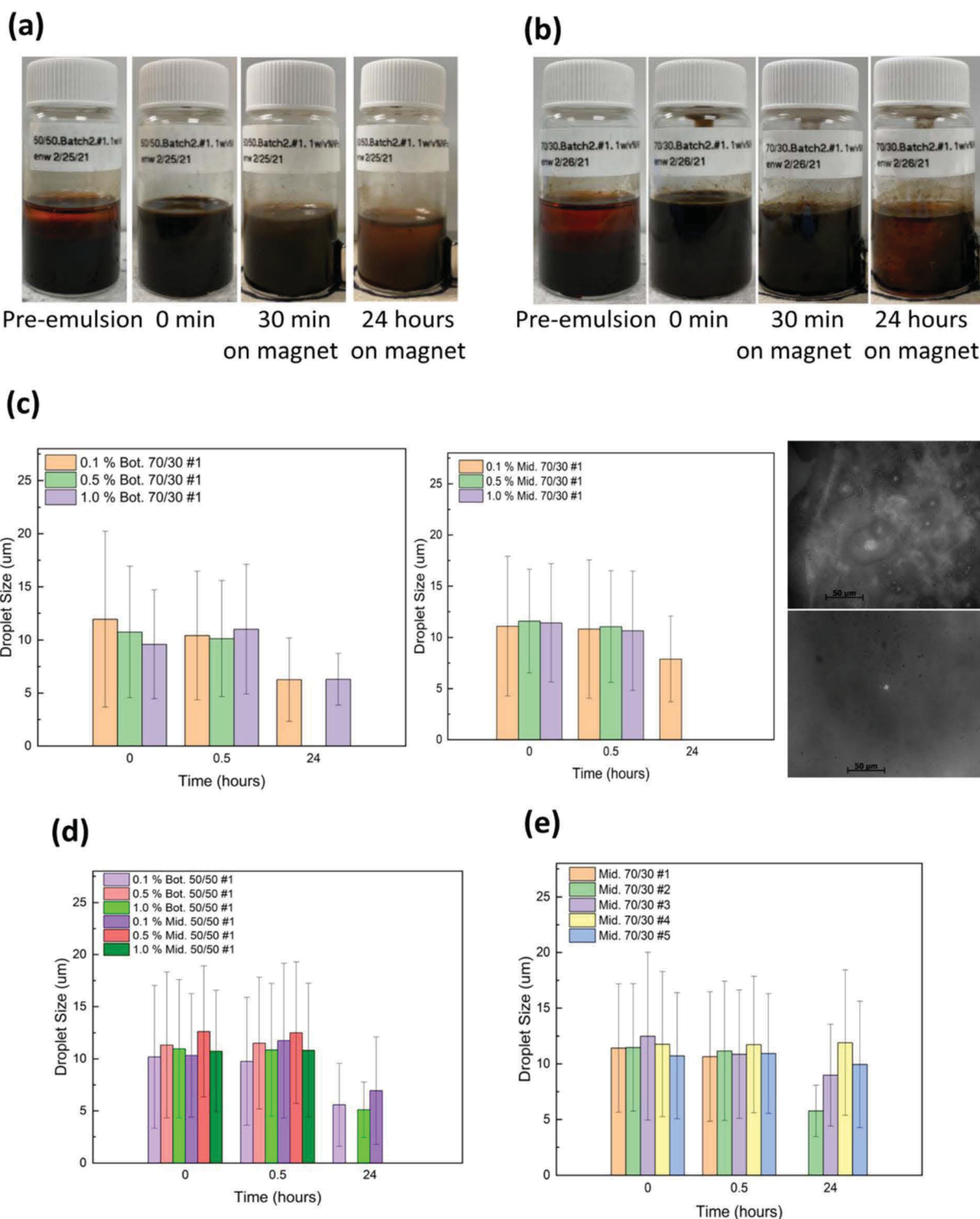


Fig. 5 Demulsification of 1 w/v% lignin@Fe₃O₄-stabilized Pickering emulsion with 540 mT magnet for the emulsions of (a) 50/50; and (b) 70/30. Average droplet size of the emulsions over 24 h at 540 mT magnetic field for the samples taken from both bottom layer and middle layer and prepared at 0.1, 0.5, and 1 w/v% and CO/W ratio of (c) 70/30 (two microscopy pictures of the emulsions at time 0 h (top) and 24 h on magnet (bottom) were also included); and (d) 50/50. (e) Average droplet size of the emulsions over 24 hours at varied magnetic fields. In the figure (top to bottom) #1 stands for 540 mT, #2 for 370 mT, #3 for 100 mT, #4 for 5 mT and #5 for 0 mT.

Videos S1 and S2†). Moreover, the effect of magnetic field on oil herding was tested by using two magnets with different intensities. The larger magnet (1 × 1 × 2 in) had a magnetic field

intensity of 60 mT at the center of the Petri dish (Fig. 6c, right), while the medium magnet (0.5 × 0.5 × 2 in) had a magnetic field of 13 mT at the center (Fig. 6c, left). It was observed that the



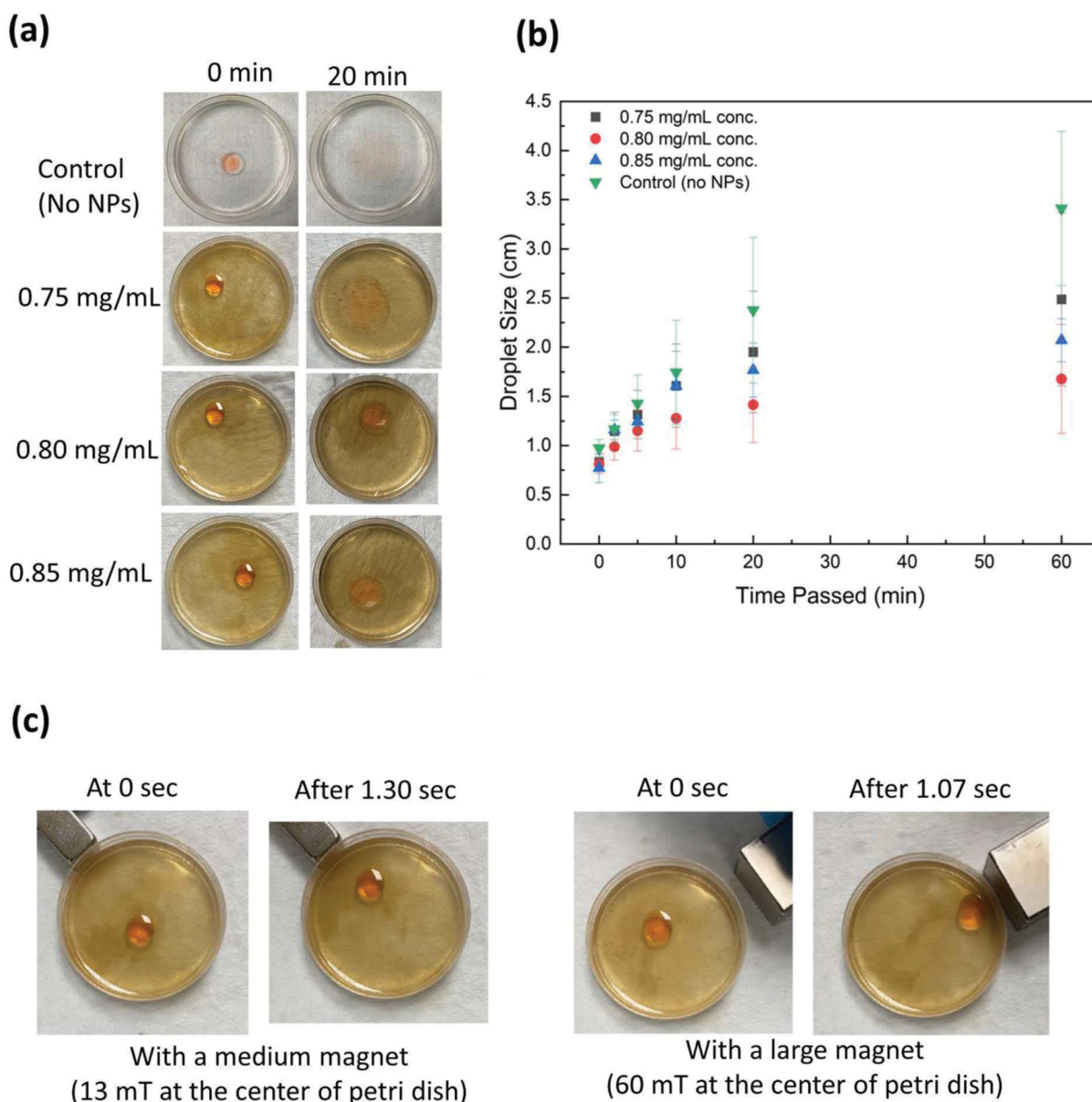


Fig. 6 (a) Herding of castor oil using lignin@Fe₃O₄ NPs at various concentration as herding agent and 1-pentanol; (b) change in size of the herded oil over time; (c) magnetic manipulation of oil herding using 0.80 mg mL⁻¹ of lignin@Fe₃O₄ loading in 1-pentanol and using two permanent magnets at different intensities.

herded oil at the center of the dish moved quicker to the larger magnet. All three NP concentrations were able to be manipulated by both magnets, but the large magnet had a larger effect. Therefore, it was concluded that the stronger the magnetic field, the faster the velocity of the herded oil.

4. Conclusions

This study demonstrated the applications of lignin@Fe₃O₄ nanoparticles in stabilizing castor oil/water emulsions, on-demand magnetic demulsification, and oil spill recovery. The lignin-coated magnetic nanoparticles were synthesized through a simple co-precipitation and pH-induced process using a 3 : 1

lignin to Fe₃O₄ mass ratio. FT-IR, XRD, TGA, TEM, and VSM showed the successful assembly of lignin and Fe₃O₄ NPs as well as their superparamagnetic properties. DLS provided an average effective nanoparticle diameter of lignin@Fe₃O₄ to be 168 ± 1.7 nm, where TEM imaging found the average diameter of the Fe₃O₄ core to be 13.4 ± 5.5 nm. The saturation magnetization of the lignin@Fe₃O₄ NPs at room temperature was measured to be ~50 emu g⁻¹, which was proven to be sufficient for their use in magnetic demulsification. Various castor oil/water ratios (10/90, 30/70, 50/50, 70/30, and 90/10) with different lignin@Fe₃O₄ NPs concentration (0.1, 0.5, and 1 w/v%) were analyzed. We found that Pickering emulsions with a higher castor oil-to-water ratio and a higher NP concentration, such as the 70/30, 1.0 w/v% NP



concentration, had the longest stability and most consistent droplet size after 24 hours. On-demand demulsification of the as-prepared Pickering emulsions were analyzed under various magnetic field strengths (540, 370, 100, 5, and 0 mT). The magnetic demulsification was stronger and faster with an increasing magnetic field strength (*e.g.*, at 540 mT). Lastly, the lignin@Fe₃O₄ nanoparticles were used as an oil herding agent where they were dispersed in aqueous suspension at varying concentrations (0, 0.75, 0.8, and 0.85 mg L⁻¹) to castor oil spill recovery in the presence of 1-pentanol. At a concentration of 0.80 mg mL⁻¹ and using 1-pentanol, lignin@Fe₃O₄ could herd spilled oil over water *via* a Marangoni flow, allowing for magnetic manipulation of the oil and nanoparticle encapsulation up to 1 h after applying the magnetic field. The applicability of the lignin@Fe₃O₄ in Pickering emulsions and oil herding could be instrumental in large-scale magnetically controlled liquid–liquid extractions and large-scale oil spill clean-up and recovery, assisting the environment in a safe and low-cost manner.

Author contributions

Mohammad Jahid Hasan: investigation, analysis, visualization, writing – manuscript, Emily Westphal: conceptualization, investigation, visualization, formal analysis, writing – original draft. Peng Chen: investigation, formal analysis, resources, visualization, writing – review & editing. I-Wei Chu: investigation, writing – review & editing. Abhishek Saini: investigation, analysis. Sarah Watzman: analysis, writing – review & editing. Esteban Urena-Benavides: conceptualization, formal analysis, writing – review & editing, funding acquisition. Erick Vasquez: conceptualization, formal analysis, resources, data curation, visualization, writing – review & editing, supervision, project administration, funding acquisition.

Conflicts of interest

There are no conflicts to declare.

Acknowledgements

This work was funded in part by the National Science Foundation under Grants 1705331 and 1704897. Additional funding was provided by the University of Dayton School of Engineering Graduate Assistant Fellowship.

References

- 1 Y.-J. Lin, A. Perrard, S. L. Biswal, R. M. Hill and S. Trabelsi, *Energy Fuels*, 2018, **32**, 4903–4910.
- 2 L. Bai, S. Lv, W. Xiang, S. Huan, D. J. McClements and O. J. Rojas, *Food Hydrocolloids*, 2019, **96**, 699–708.
- 3 S. Parajuli, A. L. Dorris, C. Middleton, A. Rodriguez, M. O. Haver, N. I. Hammer and E. Ureña-Benavides, *Langmuir*, 2019, **35**, 12061–12070.
- 4 I. A. Udoetok, L. D. Wilson and J. V. Headley, *Adv. Mater. Sci.*, 2016, **1**, 24–33.
- 5 S. Mirshahghassemi and J. R. Lead, *Environ. Sci. Technol.*, 2015, **49**, 11729–11736.
- 6 J. Philip, *Adv. Colloid Interface Sci.*, 2023, **311**, 102810.
- 7 C. Anushree, D. N. G. Krishna and J. Philip, *J. Mol. Liq.*, 2020, **320**, 114324.
- 8 C. Anushree, D. Nanda Gopala Krishna and J. Philip, *J. Mol. Liq.*, 2021, **337**, 116429.
- 9 S. Parajuli, M. J. Hasan and E. E. Ureña-Benavides, *Materials*, 2022, **15**(19), 6673.
- 10 M. J. Hasan, F. Yeganeh, A. Ciric, P. Chen, E. S. Vasquez and E. E. Urena-Benavides, *J. Chem. Thermodyn.*, 2023, DOI: [10.1016/j.jct.2023.107007](https://doi.org/10.1016/j.jct.2023.107007).
- 11 V. Poulichet and V. Garbin, *Proc. Natl. Acad. Sci.*, 2015, **112**, 5932–5937.
- 12 B. Doshi, M. Sillanpää and S. Kalliola, *Water Res.*, 2018, **135**, 262–277.
- 13 T. Mi, Y. Cai, Q. Wang, N. Habibul, X. Ma, Z. Su and W. Wu, *RSC Adv.*, 2020, **10**, 10309–10314.
- 14 H. Yang, S. Wang, W. Zhang, J. Wu, S. Yang, D. Yu, X. Wu, Y. Sun and J. Wang, *Sci. Rep.*, 2020, **10**, 16565.
- 15 C. Anushree and J. Philip, *Colloids Surf., A*, 2019, **567**, 193–204.
- 16 Z. Wang, P. Jin, M. Wang, G. Wu, C. Dong and A. Wu, *ACS Appl. Mater. Interfaces*, 2016, **8**, 32862–32868.
- 17 M. Khosravi and S. Azizian, *ACS Appl. Mater. Interfaces*, 2015, **7**, 25326–25333.
- 18 X. H. Yau, C. S. Khe, M. S. M. Saheed, C. W. Lai, K. Y. You and W. K. Tan, *PLoS One*, 2020, **15**, e0232490.
- 19 R. C. Popescu, E. Andronescu and B. S. Vasile, *Nanomaterials*, 2019, **9**, 1791.
- 20 V. Socoliuc, D. Peddis, V. I. Petrenko, M. V. Avdeev, D. Susan-Resiga, T. Szabó, R. Turcu, E. Tombácz and L. Vékás, *Magnetochemistry*, 2020, **6**, 2.
- 21 E. Tombácz, R. Turcu, V. Socoliuc and L. Vékás, *Biochem. Biophys. Res. Commun.*, 2015, **468**, 442–453.
- 22 C. Justin, S. A. Philip and A. V. Samrot, *Appl. Nanosci.*, 2017, **7**, 463–475.
- 23 M. Mahmoudi, H. Hofmann, B. Rothen-Rutishauser and A. Petri-Fink, *Chem. Rev.*, 2012, **112**, 2323–2338.
- 24 W. Daoush, *J. Nanomed. Res.*, 2017, **5**(3), 00118.
- 25 M. Calero, L. Gutiérrez, G. Salas, Y. Luengo, A. Lázaro, P. Acedo, M. P. Morales, R. Miranda and A. Villanueva, *Nanomed.: Nanotechnol. Biol. Med.*, 2014, **10**, 733–743.
- 26 M. Cîrcu, A. Nan, G. Borodi, J. Liebscher and R. Turcu, *Nanomater.*, 2016, **6**, 228.
- 27 A. Pal, V. Malik, L. He, B. H. Ern e, Y. Yin, W. K. Kegel and A. V. Petukhov, *Angew. Chem., Int. Ed.*, 2015, **54**, 1803–1807.
- 28 A. G. Kolhatkar, A. C. Jamison, D. Litvinov, R. C. Willson and T. R. Lee, *Int. J. Mol. Sci.*, 2013, **14**, 15977–16009.
- 29 M. J. Hasan, F. A. Petrie, A. E. Johnson, J. Peltan, M. Gannon, R. T. Busch, S. O. Leontsev, E. S. Vasquez and E. E. Urena-Benavides, *Cellulose*, 2021, **28**, 4807–4823.
- 30 D. Kai, M. J. Tan, P. L. Chee, Y. K. Chua, Y. L. Yap and X. J. Loh, *Green Chem.*, 2016, **18**, 1175–1200.
- 31 A. P. Richter, J. S. Brown, B. Bharti, A. Wang, S. Gangwal, K. Houck, E. A. Cohen Hubal, V. N. Paunov, S. D. Stoyanov and O. D. Velev, *Nat. Nano*, 2015, **10**, 817–823.



- 32 C. Frangville, M. Rutkevičius, A. P. Richter, O. D. Velev, S. D. Stoyanov and V. N. Paunov, *ChemPhysChem*, 2012, **13**, 4235–4243.
- 33 S. Jiang, D. Kai, Q. Q. Dou and X. J. Loh, *J. Mater. Chem. B*, 2015, **3**, 6897–6904.
- 34 C. Asada, S. Basnet, M. Otsuka, C. Sasaki and Y. Nakamura, *Int. J. Biol. Macromol.*, 2015, **74**, 413–419.
- 35 E. Fortunati, W. Yang, F. Luzi, J. Kenny, L. Torre and D. Puglia, *Eur. Polym. J.*, 2016, **7**(80), 295–316.
- 36 D. Kai, S. Jiang, Z. W. Low and X. J. Loh, *J. Mater. Chem. B*, 2015, **3**, 6194–6204.
- 37 L. Lin, Y. Li and F. K. Ko, *J. Fiber Bioeng. Inform.*, 2013, **6**, 335–347.
- 38 W.-J. Liu, H. Jiang and H.-Q. Yu, *Green Chem.*, 2015, **17**, 4888–4907.
- 39 L. Dai, Y. Li, F. Kong, K. Liu, C. Si and Y. Ni, *ACS Sustainable Chem. Eng.*, 2019, **7**, 13497–13504.
- 40 X. Li, Y. Wang, B. Wang, X. Feng, Z. Mao and X. Sui, *Int. J. Biol. Macromol.*, 2020, **144**, 624–631.
- 41 Y. Pang, S. Wang, X. Qiu, Y. Luo, H. Lou and J. Huang, *J. Agric. Food Chem.*, 2017, **65**, 11011–11019.
- 42 Y. Wang, X. Li, C. Shen, Z. Mao, H. Xu, Y. Zhong, X. Sui, X. Feng and B. Wang, *Int. J. Biol. Macromol.*, 2020, **146**, 1–8.
- 43 H. Wang, K.-Y. Lin, B. Jing, G. Krylova, G. E. Sigmon, P. McGinn, Y. Zhu and C. Na, *Water Res.*, 2013, **47**, 4198–4205.
- 44 A. V. Dudchenko, J. Rolf, L. Shi, L. Olivas, W. Duan and D. Jassby, *ACS Nano*, 2015, **9**, 9930–9941.
- 45 Y. J. Kim, Y. D. Liu, Y. Seo and H. J. Choi, *Langmuir*, 2013, **29**, 4959–4965.
- 46 J. G. Lee, L. L. Larive, K. T. Valsaraj and B. Bharti, *ACS Appl. Mater. Interfaces*, 2018, **10**, 43282–43289.
- 47 F. A. Petrie, J. M. Gorham, R. T. Busch, S. O. Leontsev, E. E. Ureña-Benavides and E. S. Vasquez, *Int. J. Biol. Macromol.*, 2021, **181**, 313–321.
- 48 Y. Li, M. Wu, B. Wang, Y. Wu, M. Ma and X. Zhang, *ACS Sustainable Chem. Eng.*, 2016, **4**, 5523–5532.
- 49 D. Kołodyńska, M. Gęca, I. V. Pylypchuk and Z. Hubicki, *Nanoscale Res. Lett.*, 2016, **11**, 152.
- 50 R. Massart, *IEEE Trans. Magn.*, 1981, **17**, 1247–1248.
- 51 F. Petrie, Magnetic-lignin Nanoparticles as Potential Ethanol Extractants from Aqueous Solutions, Thesis, University of Dayton, 2019.
- 52 B. V Farias, D. Brown, A. Hearn, N. Nunn, O. Shenderova and S. A. Khan, *J. Colloid Interface Sci.*, 2020, **580**, 180–191.
- 53 W. Yang, E. Fortunati, D. Gao, G. M. Balestra, G. Giovanale, X. He, L. Torre, J. M. Kenny and D. Puglia, *ACS Sustainable Chem. Eng.*, 2018, **6**, 3502–3514.
- 54 D. Kołodyńska, M. Gęca, I. V. Pylypchuk and Z. Hubicki, *Nanoscale Res. Lett.*, 2016, **11**, 152.
- 55 M. Ounacer, A. Essoumhi, M. Sajieddine, A. Razouk, B. F. O. Costa, S. M. Dubiel and M. Sahlaoui, *J. Supercond. Novel Magn.*, 2020, **33**, 3249–3261.
- 56 J. Abraham, B. Jose, A. Jose and S. Thomas, in *Phytonanotechnology*, 2020, pp. 21–39.
- 57 M. J. Hasan, A. E. Johnson and E. E. Ureña-Benavides, *Curr. Res. Green Sustainable Chem.*, 2021, **4**, 100081.
- 58 A. Mirzazadeh Ghanadi, A. Heydari Nasab, D. Bastani and A. A. Seife Kordi, *Chem. Eng. Commun.*, 2015, **202**, 600–605.
- 59 X. Qiao, J. Zhou, B. P. Binks, X. Gong and K. Sun, *Colloids Surf., A*, 2012, **412**, 20–28.
- 60 C. Jiménez Saelices and I. Capron, *Biomacromolecules*, 2018, **19**, 460–469.
- 61 P. Chen, S. Harmand, S. Ouenzerfi and J. Schiffler, *J. Phys. Chem. B*, 2017, **121**, 5824–5834.
- 62 J. G. Lee, L. L. Larive, K. T. Valsaraj and B. Bharti, *ACS Appl. Mater. Interfaces*, 2018, **10**, 43282–43289.

